

# K-shell energy levels and radiative rates for transitions in Si IX<sup>\*</sup>

H. G. Wei, J. R. Shi, F. L. Wang, J. Y. Zhong, G. Y. Liang, and G. Zhao

Key Laboratory of Optical Astronomy, National Astronomical Observatories, Chinese Academy of Sciences, 100012 Beijing, PR China  
e-mail: [whg; gzhao]@nao.cas.cn

Received 28 February 2014 / Accepted 13 May 2014

## ABSTRACT

**Context.** Accurate atomic data are needed to analyze the Si IX K-shell features in astrophysical X-ray spectra. Relative large discrepancies in the existing atomic data have impeded this progress.

**Aims.** We present the accurate Si IX K-shell transition data, including K-shell energy levels, wavelengths, radiative rates, and oscillator strengths.

**Methods.** The flexible atomic code (FAC), which is a fully relativistic atomic code with configuration interaction (CI) included, was employed to calculate these data. To investigate the CI effects, calculations with different configurations included were carried out.

**Results.** The K-shell atomic data of Si IX transitions between  $1s^22s^22p^2$ ,  $1s^22s2p^3$ ,  $1s^22p^4$ ,  $1s2s^22p^3$ ,  $1s2s2p^4$ , and  $1s2p^5$  are reported. The accuracy of our data is demonstrated by comparing them with the available experimental measurements and theoretical calculations. The energy levels are accurate to 3.5 eV, the wavelengths to within 15 mÅ. For most transitions, the radiative rates an accuracy of 20%. The effects of CI from high-energy configurations were investigated as well.

**Key words.** atomic data – atomic processes

## 1. Introduction

Detailed spectral structures that originate from ion K-shell transitions have been observed in various astrophysical objects with the high-resolution X-ray telescopes, such as *XMM-Newton*, *Chandra*, and *Suzaku* (Kaspi et al. 2000; Sako et al. 2001; Krongold et al. 2003; Holczer et al. 2007). While the iron K emission line exists in almost all X-ray sources (Bautista et al. 2003), K-line features from silicon have also been commonly observed (Kaspi et al. 2001, 2002; Kallman et al. 2009). Young et al. (2005) reported the detection of H-like Si absorption lines in MCG 6-30-15 and determined the outflow velocity by measuring the line blueshift. The K-lines from He-like silicon ions are useful tools for investigating the physical properties of plasmas around astro-objects, such as the stellar corona (Smith et al. 2004; Güdel et al. 2009), the warm absorbers that widely exist in active galaxy nuclei (AGNs; King et al. 2002; Ebrero et al. 2013; Krongold et al. 2003; Andrade-Velázquez et al. 2010), and the accretion winds around X-ray binaries (Juett & Chakrabarty 2008; Chang & Cui 2007). Based on the information (such as the column density, electron temperature, ionization states, wind velocity, and abundances) obtained by analysis of these high-resolution spectra, mechanisms that drive and heat plasmas can be deduced. Determining the abundance of various elements can shed light on the chemical evolution and origin of the hosting galaxy (Kallman et al. 2009). The L-shell transition lines from low-ionization ions of Si are used to identify them in UV spectra (Ebrero et al. 2013). Recently, more and more observations showed that the K-shell lines, namely  $1s-2p$  transitions, from these low-ionization ions of Si can also be found in high-resolution X-ray spectra. Kaspi et al. (2002) and Netzer et al. (2003) detected the Si VII to Si XIV K lines in spiral galaxy

NGC 3783. Holczer et al. (2010) reported Si VI to Si XIV absorption lines in the slow warm absorber of bright Seyfert 1 galaxy MCG 6-30-15. Hell et al. (2013) observed the K-shell absorption lines from Si VIII to Si XIV in the high-mass X-ray binary Cygnus X-1. More recently, Si VIII to Si XIV K lines have been detected in warm absorbers around the quasar MR 2251-178 (Reeves et al. 2013). Thus the accurate and comprehensive Si K-shell atomic data are urgently needed to model and analyze these high-resolution X-ray spectra.

Behar & Netzer (2002) calculated the wavelengths and oscillator strengths of  $1s - np$  ( $n \leq 3$ ) transitions from Li-like to F-like ions for elements of astrophysical interest Ne, Mg, Al, Si, S, Ar, Ca, and Fe with the Hebrew University Lawrence Livermore atomic code (HULLAC). Only lines with oscillator strengths greater than 0.1 are given in their work. Palmeri et al. (2008) have reported the K-shell atomic data for Ne, Mg, Si, S, Ar and Ca ions, including the level energies, wavelengths, *A*-values, and radiative and Auger widths using the codes HFR (Cowan 1981) and AUTOSTRUCTURE (Badnell 1986, 1997). The accuracy of their atomic data is accessed by comparison with the other previous theoretical works, and good agreement is achieved except for C-like ions. This disagreement can be as large as 40% on average for C-like ion radiative rates when compared with those from Chen et al. (1997). For some transitions the disagreement can even reach a factor of 2, while for Be-like or B-like ions, the differences are usually lower than 10%.

Unfortunately, the experiments on K-shell atomic data for low-ionization Si ions are very limited, particularly for Si IX. Trabert et al. (1979, 1982) measured and identified X-ray emission lines from H-like to N-like silicon ions in the beam-foil experiments. These lines mainly belong to K-shell  $2p-1s$  transitions, while lines from C-like and N-like ions are too weak to be clearly identified. In similar experiments, Mosnier et al. (1986) reported  $2p-1s$  transition lines from Si XI to Si XIV ions, but no lines from Si IX are reported in their work.

\* Full Tables 3 and 4 are only available at the CDS via anonymous ftp to [cdsarc.u-strasbg.fr](http://cdsarc.u-strasbg.fr) (130.79.128.5) or via <http://cdsarc.u-strasbg.fr/viz-bin/qcat?J/A+A/566/A105>

Faenov et al. (1994) precisely measured the wavelengths of Be-like to F-like ion K lines generated by laser-produced plasmas and calculated the wavelengths,  $A$ -values, and Auger rates with the MZ code (Vainshtein & Safronova 1978, 1980). Recently, Hell (2012) reported the measurements of K-line energies of the L-shell ions of Si using the electron beam ion trap EBIT-I at Lawrence Livermore National Laboratory to determine the Doppler shifts of these lines in Cygnus X-1.

Configuration interaction can have strong effects on K-shell atomic data calculations. Gorczyca et al. (2003, 2006) have calculated the fluorescence yields for Be-like and Li-like ions by including configuration interaction, and found large differences between their results with those from most widely used database (Kaastra & Mewe 1993), which is configuration averaged. Hasoğlu et al. (2008) have computed the K-shell  $1s2s^22p^2$  configuration fluorescence yields using the AUTOSTRUCTURE code by including the configuration interaction and relativistic effect. Their results confirmed that there are differences with the results from the database (Kaastra & Mewe 1993), and showed that these fluorescence yields are strongly LSJ dependent. Zeng & Yuan (2006) have shown that inclusion of CI from the excited configurations can improve the accuracy of the calculations of the atomic data, such as energy levels and oscillation strengths.

Here, we mainly report the K-shell atomic data of Si IX transitions between  $1s^22s^22p^2$ ,  $1s^22s2p^3$ ,  $1s^22p^4$ ,  $1s2s^22p^3$ ,  $1s2s2p^4$ , and  $1s2p^5$ . Configuration interaction and relativistic effects are included in our calculations. Especially, configuration interaction from highly excited level configurations, which used to be neglected, are investigated. Details of calculations are described in Sect. 2. The assessments of the calculated results and discussions are then given in Sect. 3, and two supplementary tables are presented as well. The summary and conclusions are drawn in Sect. 4.

## 2. Calculations

We used the flexible atomic code (FAC), which is developed by Gu (2003), to calculate the Si IX K-shell atomic data. FAC is a fully relativistic atomic code using a modified Dirac-Fock-Slater central filed potential and takes configuration interaction into account. The radial orbitals are optimized to a fictitious mean configuration with fractional occupation numbers to represent the electronic screening effect. The configuration's average energy determined using these orbitals is different from that using the orbitals individually optimized to each specific configuration, and the difference between the two is then used to correct the final level energies. Similarly as Wei et al. (2010), these level energy-corrected procedures are employed in our FAC calculations.

The effects of configuration interaction from high-energy configurations have been investigated in iron K-shell data by Bautista et al. (2003) and Palmeri et al. (2003), who found that the configurations with  $n = 3$  have little effect on the accuracy of the  $1s-2p$  transition atomic data from Fe XVIII to Fe XXV, either for energy levels or for radiative rates. For example, differences lower than 2% are found for radiative rates when the  $n = 3$  configurations are included in Fe XXIV (Bautista et al. 2003). Hasoğlu et al. (2008) found that these configurations can only induce changes lower than 5% in K-shell radiative rates for  $1s2s^22p^3$  isoelectronic sequence. Aggarwal et al. (2006) recalculated the Fe IX data with the codes FAC and the general purpose relativistic atomic structure package (GRASP; Dyall 1989), and large differences are found when comparing their results with those from Verma et al. (2006). This arises because

CI effects from the  $3s^23p^33d^3$  configurations have been included in the calculations of Aggarwal et al. (2006), but were not included in those of Verma et al. (2006). Forster & Testa (2011) confirmed the importance of including CI effects from high-level configurations using the code FAC in Fe IX calculations, and showed that further improvements in energy levels and level orderings can be achieved by including more configurations, e.g.  $n = 6$  configurations. To evaluate the CI effects of configurations from high-energy levels, we calculated the Si IX K-shell atomic data with different configurations included. Basic configurations include  $1s^22s^22p^2$ ,  $1s^22s2p^3$ ,  $1s^22p^4$ ,  $1s2s^22p^3$ ,  $1s2s2p^4$ , and  $1s2p^5$ , referred to as FAC1. In addition to these configurations included in FAC1, we took  $n = 3$  configurations into account in FAC2 calculations, namely  $1s2s^22p^23l$ ,  $1s2s2p^33l$ , and  $1s2p^43l$ . Similarly, we involved all configurations in FAC2 and  $1s2s^22p^24l$ ,  $1s2s2p^34l$ , and  $1s2p^44l$  in FAC3 calculation. In FAC4,  $1s2s^22p^25l$ ,  $1s2s2p^35l$ , and  $1s2p^45l$  were added compared to FAC3. For FAC5, we took those  $n = 6$  configurations into consideration, namely  $1s2s^22p^26l$ ,  $1s2s2p^36l$ , and  $1s2p^46l$  in addition to FAC4. For the largest calculations of FAC6, some double-excited configurations of  $1s2s^22p^3l^2$ ,  $1s2s2p^23l^2$ , and  $1s2p^33l^2$  were included in addition to the configurations in FAC5.

## 3. Results and discussion

Assessments on the accuracy of our calculated atomic data can be done by comparing our results with those of the previous theoretical and experimental atomic data. The effects of CI from high energy configurations are also discussed in the following sections.

### 3.1. Energy levels and wavelengths

We present our calculated energy levels with FAC1 and FAC6 in Table 1, where FAC1 and FAC6 are the results with the smallest and largest configurations included. The calculated energy levels from FAC1 to FAC6 are compared, and Fig. 1 shows the energy differences between FAC6 and the other calculated results, namely FAC1, FAC2, FAC3, FAC4, and FAC5, to investigate the impact of CI from high-energy configurations. With more and more configurations included, the energy differences between FAC6 and other calculated results decrease. The highest and the mean energy difference between FAC6 and FAC1 are 3.3 eV and 1.3 eV. The differences between FAC6 and FAC5 are reduced to 0.3 eV and 0.1 eV. Considerable impact on the energy level values is observed when the  $n = 3$  configurations are included in FAC2, which reduces the energy differences between FAC2 and FAC6 to approximately 1 eV. The reason is that the energy levels belonging to  $n = 3$  configurations closely interact with  $n = 2$  configurations since the energies of all these levels are very close. This also suggests that CI from the configurations of higher energy levels has weaker effects on the atomic data calculations because these levels are much higher than the levels considered here. That is why the calculations converge. In Table 1, we also list the calculated energy levels from Palmeri et al. (2008, hereafter HFR1). They have employed the code HFR (Cowan 1981) and took the relativistic corrections except two-body Breit interaction into consideration. The configurations considered in their work are the same as in our FAC1. The energy differences between FAC1 and HFR1 are lower than 1.5 eV, as shown in Fig. 1. However, these differences can reach as much as 3.5 eV between FAC6 and HFR1. Since the same configurations have been considered in FAC1 and HFR1, the differences are relative small. The main reason

**Table 1.** Comparison of level energies for Si IX.

Index	Level configurations	FAC6	FAC1	HFR1	NIST
1	$1s^2 2s^2 2p^2 \ ^3P_0$	0.0000	0.0000	0.0000	0.0000
2	$1s^2 2s^2 2p^2 \ ^3P_1$	0.3110	0.3110	0.3103	0.3155
3	$1s^2 2s^2 2p^2 \ ^3P_2$	0.7843	0.7842	0.8186	0.7952
4	$1s^2 2s^2 2p^2 \ ^1D_2$	6.9119	6.9092	6.9421	6.5620
5	$1s^2 2s^2 2p^2 \ ^1S_0$	13.1139	13.0982	13.3095	13.3654
6	$1s^2 2s 2p^3 \ ^5S_2^o$	17.1867	17.1885	17.7041	18.6930
7	$1s^2 2s 2p^3 \ ^3D_3^o$	36.5918	36.6003	36.6691	36.2322
8	$1s^2 2s 2p^3 \ ^3D_2^o$	36.5996	36.6081	36.6354	36.2401
9	$1s^2 2s 2p^3 \ ^3D_1^o$	36.6166	36.6251	36.6408	36.2581
10	$1s^2 2s 2p^3 \ ^3P_1^o$	42.9876	42.9907	43.0605	42.6517
•11	$1s^2 2s 2p^3 \ ^3P_2^o$	42.9882	42.9912	43.0827	42.6652
•12	$1s^2 2s 2p^3 \ ^3P_0^o$	43.0001	43.0032	43.0488	42.6599
13	$1s^2 2s 2p^3 \ ^1D_2^o$	56.4180	56.4480	56.1320	54.6030
14	$1s^2 2s 2p^3 \ ^3S_1^o$	56.7579	56.8027	56.6580	55.4138
15	$1s^2 2s 2p^3 \ ^1P_1^o$	62.7986	62.8230	62.5962	61.0939
16	$1s^2 2p^4 \ ^3P_2$	85.0797	85.1174	84.8570	83.6601
17	$1s^2 2p^4 \ ^3P_1$	85.6402	85.6778	85.3876	84.2200
18	$1s^2 2p^4 \ ^3P_0$	85.8237	85.8611	85.6127	84.4431
19	$1s^2 2p^4 \ ^1D_2$	91.7466	91.7814	91.0718	89.2069
20	$1s^2 2p^4 \ ^1S_0$	104.6293	104.6604	103.8140	101.6285
21	$1s 2s^2 2p^3 \ ^5S_2^o$	1770.4975	1773.7723	1773.8817	
22	$1s 2s^2 2p^3 \ ^3D_2^o$	1784.7499	1787.4198	1788.2761	
23	$1s 2s^2 2p^3 \ ^3D_1^o$	1784.8997	1787.5480	1788.1941	
24	$1s 2s^2 2p^3 \ ^3D_3^o$	1784.9242	1787.5755	1788.1998	
25	$1s 2s^2 2p^3 \ ^3S_1^o$	1788.4156	1790.7066	1791.5719	
26	$1s 2s^2 2p^3 \ ^3P_0^o$	1789.2415	1791.4397	1792.4497	
27	$1s 2s^2 2p^3 \ ^3P_2^o$	1789.3511	1791.5274	1792.4240	
28	$1s 2s^2 2p^3 \ ^3P_1^o$	1789.4253	1791.6428	1792.6255	
29	$1s 2s^2 2p^3 \ ^1D_2^o$	1793.9727	1796.1568	1797.2570	
30	$1s 2s^2 2p^3 \ ^1P_1^o$	1798.3268	1800.0376	1801.3853	
31	$1s(2S)2s2p^4(4P) \ ^5P_3$	1802.5020	1804.8182	1804.7629	
32	$1s(2S)2s2p^4(4P) \ ^5P_2$	1803.1056	1805.4265	1805.2733	
33	$1s(2S)2s2p^4(4P) \ ^5P_1$	1803.4485	1805.7751	1805.5979	
34	$1s(2S)2s2p^4(4P) \ ^3P_2$	1822.8326	1824.4463	1824.9594	
•35	$1s(2S)2s2p^4(4P) \ ^3P_1$	1823.3024	1824.9486	1825.8293	
•36	$1s(2S)2s2p^4(2D) \ ^3D_3$	1823.4531	1825.6564	1825.8344	
37	$1s(2S)2s2p^4(4P) \ ^3P_0$	1823.6638	1825.8244	1825.6722	
•38	$1s(2S)2s2p^4(2D) \ ^3D_1$	1823.6697	1825.2575	1825.7697	
•39	$1s(2S)2s2p^4(2D) \ ^3D_2$	1823.7625	1825.8952	1825.3947	
40	$1s(2S)2s2p^4(2S) \ ^3S_1$	1833.6867	1835.3161	1835.7917	
41	$1s(2S)2s2p^4(2D) \ ^1D_2$	1836.4113	1838.2599	1838.9041	
42	$1s(2S)2s2p^4(2P) \ ^3P_2$	1838.2168	1840.6016	1840.4812	
43	$1s(2S)2s2p^4(2P) \ ^3P_1$	1838.7842	1841.1781	1840.9210	
44	$1s(2S)2s2p^4(2P) \ ^3P_0$	1838.9370	1841.3274	1841.0937	
45	$1s(2S)2s2p^4(2P) \ ^1P_1$	1845.7907	1847.8227	1847.5927	
46	$1s(2S)2s2p^4(2S) \ ^1S_0$	1846.7293	1848.0086	1849.1591	
47	$1s 2p^5 \ ^3P_2^o$	1869.2117	1871.5190	1870.9739	
48	$1s 2p^5 \ ^3P_1^o$	1869.8556	1872.1694	1871.5886	
49	$1s 2p^5 \ ^3P_0^o$	1870.3230	1872.6383	1871.9329	
50	$1s 2p^5 \ ^1P_1^o$	1878.3528	1880.3785	1879.8982	

**Notes.** FAC6: level energies computed by largest configurations included in the FAC code. FAC1: level energies computed by only  $n = 2$  configurations included in the FAC code. HFR1: level energies computed by only  $n = 2$  configurations included in the HFR code from Palmeri et al. (2008). NIST: level energies compiled in the NIST database (Ralchenko et al. 2013). •: level orderings changed compared to the results of Palmeri et al. (2008).

for the large differences between FAC6 and HFR1 are that the CI effects from the high-energy configurations have been included in FAC6. This phenomenon also occurred in our previous work on Si XI (Wei et al. 2010). The compiled energy levels from the NIST database (Ralchenko et al. 2013) are also listed in Table 1 (hereafter NIST). Only the levels from ground configurations, namely the lowest 20 levels in our calculated levels, are available. The differences between NIST and FAC1 are lower than

3.1 eV, which is the same as the differences between NIST and FAC6. This is because CI have little effect on the energy levels belonging to ground configurations, and the strongest energy changes caused by this effect are lower than 0.05 eV, as shown in Fig. 1. Based on these comparisons, we conclude that our FAC6 energy levels are accurate to 3.5 eV, which is higher than that in our Be-like Si XI work (Wei et al. 2010) because of the complex electron structures and interactions in C-like Si IX. The level

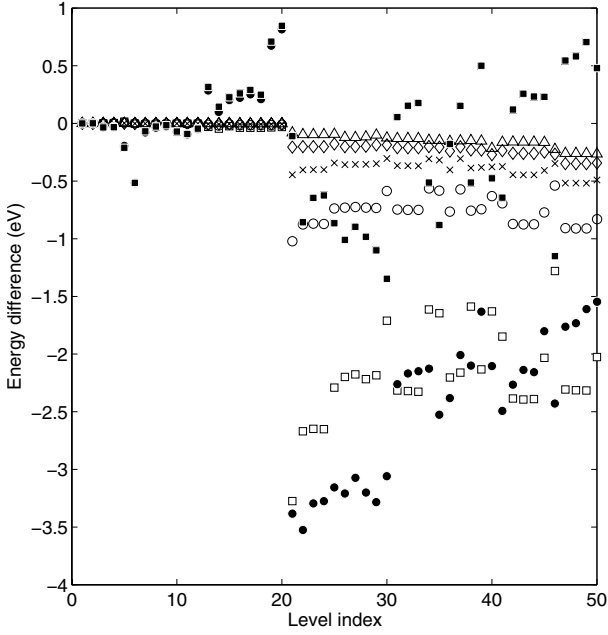


**Fig. 1.** Energy differences between our FAC calculations and the HFR1 results. The level energy differences are plotted versus the level index. Open squares: FAC6 minus FAC1. Open circles: FAC6 minus FAC2. Cross: FAC6 minus FAC3. Open diamonds: FAC6 minus FAC4. Open triangles: FAC6 minus FAC5. Solid circles: FAC6 minus HFR1 (Palmeri et al. 2008). Solid squares: FAC1 minus HFR1 (Palmeri et al. 2008).

ordering can also be altered when more configurations are included. For example, levels 11 and 12 in our results are ordered differently from NIST, while levels 10 to 12 are also differently ordered from NIST in HFR1 (Palmeri et al. 2008). Levels 35, 36, 38, and 39 would change the ordering with more configurations included, as noted in Table 1.

Experimental investigations of Si IX K-shell spectra are difficult in the laboratory. As stated in the introduction, no isolated lines of Si IX were observed using beam-foil methods (Trabert et al. 1979, 1982; Mosnier et al. 1986). The main reasons are that it is difficult to generate these K-vacancy states since the needed energies are usually higher than the ion ionization energy, and the high auto-ionization rates of these K-vacancy states depress the production of fluorescence yielding, thus these K-lines from Si IX are relatively very weak. The available experimental measurements by Faenov et al. (1994) are listed in Table 2. The largest wavelength difference between our FAC6 calculations and those of the experimental results is 8 mÅ, which is consistent with our former work on Si XI (Wei et al. 2010). Theoretical calculations from Palmeri et al. (2008) with the code HFR are also listed in Table 2, labeled HFR1. The wavelength differences between their results and those of the experimental measurements are lower than 10 mÅ, which is similar to our results. The theoretical results from Chen et al. (1997), based on a multi-configuration Dirac-Fock (MCDF) method, are listed in Table 2. Relative larger wavelength differences, which can be as large as 35 mÅ, are found when comparing their results with those of the experimental measurements, which suggests that our works are more consistent with those of Palmeri et al. (2008).

It is also interesting to compare our results with those of the above theoretical calculations for all the transition wavelengths. The wavelength differences between our results (FAC1 and FAC6) and HFR1 (Palmeri et al. 2008) are shown in Fig. 2.

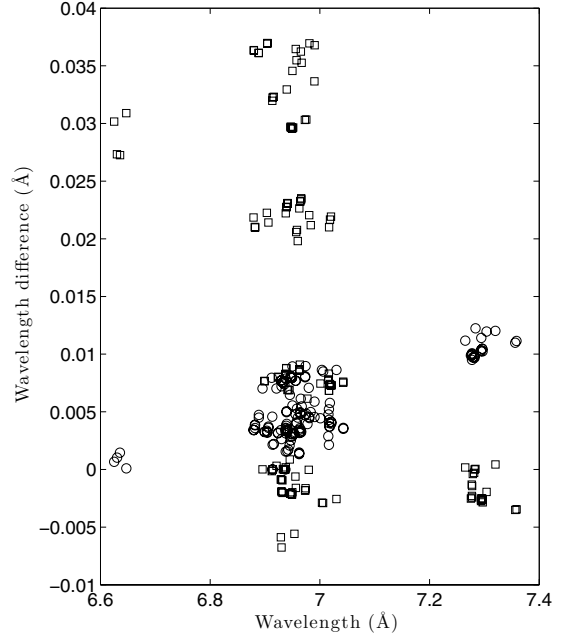


**Fig. 2.** Wavelength differences between our FAC calculations, HFR1 results, and the results from the MCDF method. The wavelength differences are plotted versus FAC6 wavelengths in Å for Si IX. Diamonds: FAC1 with HFR1 (Palmeri et al. 2008). Circles: FAC6 with HFR1 (Palmeri et al. 2008). Squares: FAC6 with MCDF method (Chen et al. 1997).

The largest wavelength difference between FAC6 and HFR1 is lower than 13 mÅ, while the difference between FAC1 and HFR1 is lower than 8 mÅ. The average wavelength difference between FAC6 and HFR1 is  $5 \text{ mÅ} \pm 2.9 \text{ mÅ}$ , while it is  $3 \pm 2.4 \text{ mÅ}$  between FAC1 and HFR1. The FAC6 wavelengths generally agree with HFR1, while the agreement between FAC1 and HFR1 is even better. This is because the CI effects from high-energy configurations have not been included in either the FAC1 or HFR1 calculations, as discussed above for energy levels. As shown in Fig. 2, large wavelength differences are found when comparing FAC6 with those from Chen et al. (1997). The largest wavelength difference is 37 mÅ and the average difference is 12 mÅ with a large standard deviation 13.8 mÅ. This big discrepancy is beyond the error ranges of our FAC6 or HFR1. Behar & Netzer (2002) have presented the strongest transition line for C-like Si IX is 6.939 Å in wavelength, which also agrees well with our FAC6, and the difference is only 1 mÅ. By comparison with both experimental and previous theoretical results, we conclude that the wavelength of our FAC6 are with an accuracy about 15 mÅ.

### 3.2. Radiative rates

Before we tested the accuracy of our radiative rates, we investigated the CI effects from configurations of high-energy levels. Detailed comparison were carried out on the radiative rates between our FAC1, FAC2, FAC3, FAC4, FAC5, and FAC6 calculations. Only the ratios for the strong transition rates ( $> 1E+13 s^{-1}$ ) are shown in Fig. 3. All transitions whose upper levels belongs to configurations  $1s2s^22p^3$  and  $1s2p^5$ , agree well within 5%, except for two transitions within 20%. This indicates that even if more configurations included, the CI effects on radiative rates can be neglected. These results agree with the findings of

**Table 2.** Wavelengths of K-shell transitions in Si IX

Index	Upper level( $J^\pi$ )	Lower level( $J^\pi$ )	$\lambda^a$	$\lambda^b$	$\lambda^c$	$\lambda^d$ (Å)
1	$1s2s^22p^3\ ^3P_1^o$	$1s^22s^22p^2\ ^3P_1$	6.924	6.930	6.922	6.931
2	$1s2s^22p^3\ ^3S_1^o$	$1s^22s^22p^2\ ^3P_1$	6.927	6.933	6.926	6.934
3	$1s2s^22p^3\ ^1D_2^o$	$1s^22s^22p^2\ ^1D_2$	6.932	6.938	6.930	6.938
4	$1s2s2p^4\ ^3D_3$	$1s^22s2p^3\ ^3D_2^o$	6.938	6.939	6.935	6.930
5	$1s2s2p^4\ ^3P_2$	$1s^22s2p^3\ ^3D_3^o$	6.939	6.941	6.938	6.918
6	$1s2p^5\ ^1P_1^o$	$1s^22p^4\ ^1D_2$	6.941	6.940	6.936	6.907
7	$1s2s^22p^3\ ^1P_1^o$	$1s^22s^22p^2\ ^1S_0$	6.945	6.945	6.939	6.944
8	$1s2p^5\ ^3P_2^o$	$1s^22p^4\ ^3P_2$	6.950	6.947	6.945	6.917
9	$1s2p^5\ ^3P_2^o$	$1s^22p^4\ ^3P_2$	6.952	6.954	6.951	6.959
10	$1s2s2p^4\ ^3P_1$	$1s^22s2p^3\ ^3S_1^o$	6.955	6.958	6.954	6.922
11	$1s2s2p^4\ ^1D_2$	$1s^22s2p^3\ ^1D_2^o$	6.960	6.965	6.959	6.929
12	$1s2s2p^4\ ^3D_3$	$1s^22s2p^3\ ^3P_2^o$	6.962	6.964	6.960	6.956
13	$1s2s2p^4\ ^1D_2$	$1s^22s2p^3\ ^1P_1^o$	6.985	6.991	6.985	6.958
14	$1s2p^5\ ^1P_1^o$	$1s^22p^4\ ^1S_0$	6.991	6.990	6.986	6.956
15	$1s2s2p^4\ ^3P_2$	$1s^22s2p^3\ ^3D_3$	6.883	6.882	6.878	6.861
16	$1s2s^22p^3\ ^1P_1$	$1s^22s^22p^2\ ^1D_2$	6.913	6.921	6.914	6.920

**Notes.**  $\lambda^a$ : Laser plasma experimental results from Faenov et al. (1994).  $\lambda^b$ : our FAC6 calculations.  $\lambda^c$ : calculations with HFR (Palmeri et al. 2008).  $\lambda^d$ : calculations with MCDF (Chen et al. 1997).

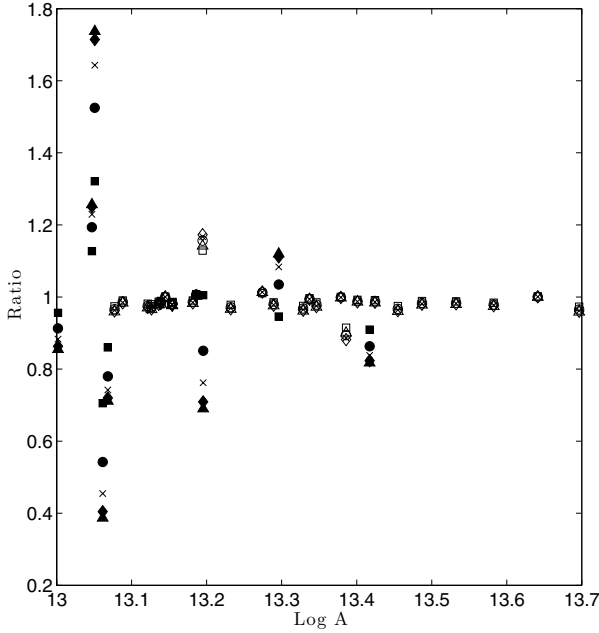


**Fig. 3.** Comparison of radiative rates between different FAC calculations. The ratio is plotted versus the FAC6 radiative rates. Squares: FAC6/FAC1. Circles: FAC6/FAC2. Cross: FAC6/FAC3. Diamond: FAC6/FAC4. Triangle: FAC6/FAC5. Solid dots are transitions originating from levels 34, 35, 38, and 39.

Hasoğlu et al. (2008). They used the multiconfiguration Breit-Pauli (MCBP) method to calculate radiative rates for  $1s2s^22p^3$  isoelectronic sequence, and found changes lower than 5% in radiative rates by including  $n = 3$  configurations. However, large changes are found for transitions belonging to the configuration  $1s2s2p^4$ . In Fig. 3, the transition rates from levels 34, 35, 38, and 39, which belong to configuration  $1s2s2p^4$ , can change by as much as 75% between FAC1 and FAC6. These differences are gradually reduced to be lower than 5% with more extensive configurations included. Similarly to the energy levels, distinct changes occur in radiative rates when  $n = 3$  configurations are taken into account in the calculations, since energy levels from

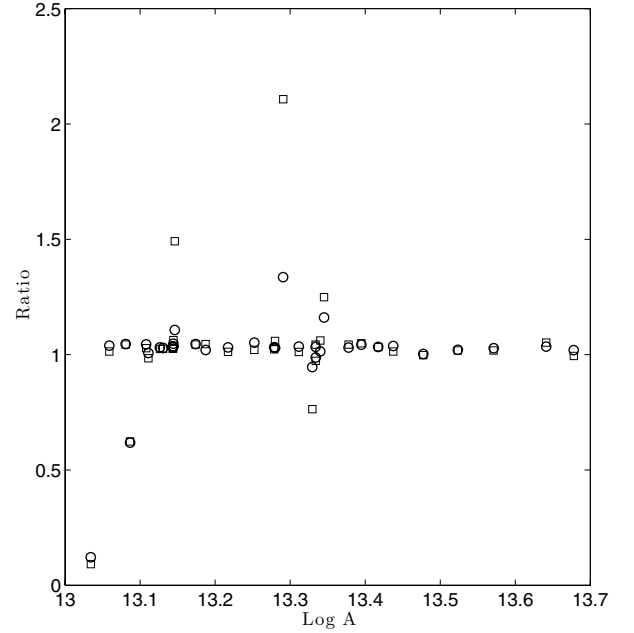


**Fig. 4.** Comparison of radiative rates between FAC6 and the results from HFR1 and FAC1. Squares: HFR1 (Palmeri et al. 2008). Circles: FAC1 (with radiative rates higher than  $1E + 13(s^{-1})$ ).

both  $n = 2$  and  $n = 3$  configurations are very similar and CI effects are strong. Thus, our results show that the configurations from high-energy levels have strong CI effects on transitions from  $1s2s2p^4$  configurations in Si IX and need to be included in atomic calculations.

To assess the accuracy of our FAC6 calculations, comparisons of our results with those from Palmeri et al. (2008) were carried out for the strong transitions ( $>1E + 13s^{-1}$ ). In our previous Be-like Si XI work, results calculated with the FAC code and those from Palmeri et al. (2008) agreed well for these strong transitions (within 10%). As shown in Fig. 4, for C-like Si IX, most radiative rates agree well with those from Palmeri et al. (2008), and the differences are lower than 10%. Large discrepancies exist both between FAC1 and HFR1 and between FAC6

**Table 3.** Level energies of K-shell transitions for Si IX.

Index	Configurations	$J^\pi$	Energy (eV)
1	1s22s22p(1/2)2	0(e)	0.0000
2	1s22s22p(1/2)2p(3/2)	1(e)	0.3110
3	1s22s22p(3/2)2	2(e)	0.7843
4	1s22s22p(1/2)2p(3/2)	2(e)	6.9119
5	1s22s22p(3/2)2	0(e)	13.1139
6	1s22s2p(1/2)2p(3/2)2	2(o)	17.1867
7	1s22s2p(1/2)2p(3/2)2	3(o)	36.5918
8	1s22s2p(1/2)2p(3/2)2	2(o)	36.5996

**Notes.** The complete table is available at the CDS.

and HFR1 for transitions originating from levels 34, 35, 38, and 39. The differences between FAC6 and HFR1 can be partly explained by the different configurations taken into account in the calculations, and the main reason for these differences is the relativistic effects. The levels 34 ( $1s(2S)2s2p^4(4P)^3P_2$ ) and 39 ( $1s(2S)2s2p^4(2D)^3D_2$ ) do not couple to each other in non-relativistic conditions. However, these two levels show strong relativistic interactions through spin-orbit interaction because of the same angular momentum  $J = 1$  and the very similar energy values. Thus, the perturbation methods may not fully account for these relativistic effects. A similar explanation is valid for levels 35 ( $1s(2S)2s2p^4(4P)^3P_1$ ) and 38 ( $1s(2S)2s2p^4(2D)^3D_1$ ). For the weak transitions, as pointed out by Aggarwal et al. (2006), large differences commonly exist because of their sensitivities to the mixing coefficients. In total, 71% transitions have radiative rates within 20% between FAC6 and HFR1. By comparison with the radiative rates listed by Chen et al. (1997), we find large scatter even for the strong transitions, and most of them exceed 50%, which is not surprising since a good agreement is found between our FAC6 results with those from Palmeri et al. (2008). Inappropriate choice of the orbital wave function may be the reason for this discrepancy (Hasoğlu et al. 2008). In fact, we calculated the radiative rates with a purposely incorrect wave functions, and found a change of more than 20% in radiative rates.

### 3.3. Supplementary electronic tables

Two electronic tables are supplied at CDS as a supplement to this paper. In Table 3, state configurations, total angular quantum number, and parity of FAC6 are presented. In Table 4, the upper and lower level index are tabulated together with wavelengths, radiative rates, and absorption oscillator strengths.

## 4. Summary and conclusions

We have calculated the energy levels, wavelengths, radiative rates, and oscillator strengths for the K-shell transitions of Si IX using the relativistic atomic code FAC (Gu 2003). The accuracy of the atomic data was assessed by detailed comparison with those of previous theoretical and experimental results. Our energy levels, wavelengths, and radiative rates are in generally closer to the results from Palmeri et al. (2008), while large differences in wavelengths and radiative rates were found when comparing our results with those from Chen et al. (1997). The large differences may be due to the inappropriate choice of the wave functions. Our energy levels are accurate to 3.5 eV and the wavelengths are accurate to within 15 mÅ. The radiative rates have an accuracy of 20% for most transitions. Our conclusions

**Table 4.** K-shell transitions of Si IX

$u$	$l$	Wavelength(Å)	$A$	$f_{lu}$
21	2	7.0040	6.12e+09	7.51e-05
21	3	7.0059	1.31e+10	9.65e-05
21	4	7.0302	1.91e+08	1.41e-06
21	16	7.3563	1.28e+08	1.04e-06
21	17	7.3587	3.82e+07	5.17e-07
22	3	6.9499	1.39e+13	1.41e-01
22	4	6.9739	5.42e+10	5.53e-04
22	16	7.2946	2.10e+11	2.34e-03
23	2	6.9475	1.20e+13	1.45e-01

**Notes.** The complete table is available at the CDS.

are supported from comparing our results with the compiled experimental level data from NIST. For the wavelengths, the differences with those of laser experimental measurements (Faenov et al. 1994) are lower than 8 mÅ. The large differences of radiative rates for some strong transitions, such as level 34 and 35, are mainly due to the strong spin-orbit interactions between these levels, which suggests that it is important to include relativistic effects in calculations.

The effects of CI from high-energy configurations were investigated. For  $1s2s^22p^3$  and  $1s2p^5$  configurations of Si IX, this effect can be neglected, while for  $1s2s2p^4$  configurations, significant changes are found, e.g. as large as 75% in radiative rates. We showed that including the configurations of high-energy levels, especially  $n = 3$  configurations, is very important in Si IX K-shell data calculations.

*Acknowledgements.* This work was supported by National Basic Research Program of China (973 Program) under grant 2013CBA01503 and the National Natural Science Foundation of China under grants Nos. 11103040, 11390371, 11173032, 11273032, 11273033, 11135012, and 11220101002.

## References

- Aggarwal, K. M., Keenan, F. P., Kato, T., & Murakami, I. 2006, A&A, 460, 331  
 Andrade-Velázquez, M., Krongold, Y., Elvis, M., et al. 2010, ApJ, 711, 888  
 Badnell, N. R. 1986, J. Phys. B, 19, 3827  
 Badnell, N. R. 1997, J. Phys. B, 30, 1  
 Bautista, M. A., Mendoza, C., Kallman, T. R., & Palmeri, P. 2003, A&A, 403, 339  
 Behar, E., & Netzer, H. 2002, ApJ, 570, 165  
 Chang, Chulhoon, Cui, & Wei 2007, ApJ, 663, 1207  
 Chen, M. H., Reed, K. J., McWilliams, D. M., et al. 1997, At. Data Nucl. Data Tables, 65, 289  
 Cowan, R. D. 1981, The Theory of Atomic Structure and Spectra Berkeley: Univ. California Press  
 Dylla, K. G., Grant, I. P., Johnson, C. T., Parpia, F. A., & Plummer, E. P. 1989, Comput. Phys. Commun., 55, 424  
 Ebrero, J., Kaastra, J. S., Kriss, G. A., et al. 2013, MNRAS, 435, 3028  
 Faenov, A. Ya., Pikuz, S. A., & Shlyaptseva, A. S. 1994, Phys. Scr., 49, 41  
 Foster, A. R., & Testa, P. 2011, ApJ, 740, 52  
 Gorczyca, T. W., Kodituwakku, C. N., Korista, et al. 2003, ApJ, 592, 636  
 Gorczyca, T. W., Dumitriu, I., Hasoğlu, M. F., et al. 2006, ApJ, 638, 121  
 Güdel, M., & Naze, Y. 2009, A&ARv, 17, 309  
 Gu, M. F., 2003, ApJ, 582, 1241  
 Hell, N. 2012, Laboratory astrophysics: investigating the mystery of low charge states of Si and S in the HMXB Cyg X-1 Masters Thesis Dr Karl Remeis-Sternwarte, Universität Erlangen-Nürnberg  
 Hell, N., Miškovičová, I., Brown, G. V., et al. 2013, Phys. Scr., 156, 014008  
 Holczer, T., Behar, E., & Kaspi, S. 2007, ApJ, 663, 799  
 Holczer, T., Behar, E., & Kaspi, S. 2010, ApJ, 708, 981  
 Hasoğlu, M. F., Nikoli, D., Gorczyca, T. W., et al. 2008, Phy. Rev. A, 78, 2509  
 Juett, A. M., & Chakrabarty, D. 2006, ApJ, 646, 493  
 Kaastra, J. S., & Mewe, R. 1993, A&AS, 97, 443  
 Kallman, T. R., Bautista, M. A., Goriely, S., et al. 2009, ApJ, 701, 865  
 Kaspi, S., Brandt, W. N., Netzer, H., et al. 2000, ApJ, 535, L17

- Kaspi, Shai, Brandt, W. N., Netzer, H., et al. 2001, *ApJ*, 554, 216
- Kaspi, S., Brandt, W. N., George, I. M., et al. 2002, *ApJ*, 574, 643
- King, A. L., Miller, J. M., & Raymond, J. 2012, *ApJ*, 746, 2
- Kramida, A., Ralchenko, Yu., Reader, J., and NIST ASD Team 2013, NIST Atomic Spectra Database (ver. 5.1), Available: <http://physics.nist.gov/asd> [2013, December 31], National Institute of Standards and Technology, Gaithersburg, MD
- Krongold, Y., Nicastro, F., Brickhouse, N. S., et al. 2003, *ApJ*, 597, 832
- Mosnier, J. P., Barchewitz, R., Senemaud, C., Cukier, M., & Dei-Cas, R. 1986 *J. Phys. B: At. Mol. Opt. Phys.*, 19, 2531
- Netzer, H., Kaspi, S., Behar, E., et al. 2003, *ApJ*, 599, 933
- Palmeri, P., Mendoza, C., Kallman, T. R., & Bautista, M. A. 2003, *A&A*, 403, 1175
- Palmeri, P., Quinet, P., Mendoza, C., et al. 2008, *ApJS*, 177, 408
- Reeves, J. N., Porquet, D., Braitto, V., et al. 2013, *ApJ*, 776, 99
- Sako, M., Kahn, S. M., Behar, E., et al., 2001, *A&A*, 365, L168
- Safronova, U. I., & Urnov, A. M. 1979, *J. Phys. B: At. Mol. Opt. Phys.*, 12, 3171
- Smith, M. A., Cohen, D. H., Gu, M. F., et al. 2004, *ApJ*, 600, 972
- Trabert, E., Armour, I. A., Bashkin, S., et al. 1979, *J. Phys. B: At. Mol. Opt. Phys.*, 12, 1665
- Trabert, E., Fawcett, B. C., & Silver, J. D. 1982 *J. Phys. B: At. Mol. Opt. Phys.*, 15, 3587
- Vainshtein, L. A., & Safronova, U. I. 1978, *At. Data Nucl. Data Tables*, 21, 49
- Vainshtein, L. A., & Safronova, U. I. 1980, *At. Data Nucl. Data Tables*, 25, 311
- Verma, N., Jha, A. K. S., & Mohan, M. 2006, *ApJS*, 164, 297
- Wei, H. G., Shi, J. R., Zhao, G., et al. 2010, *A&A*, 522, A103
- Young, A. J., Lee, J. C., Fabian, A. C., et al. 2005, *ApJ*, 631, 733
- Zeng, Jiaolong, & Yuan, Jianmin. 2006, *Phy. Rev. E*, 74, 5401